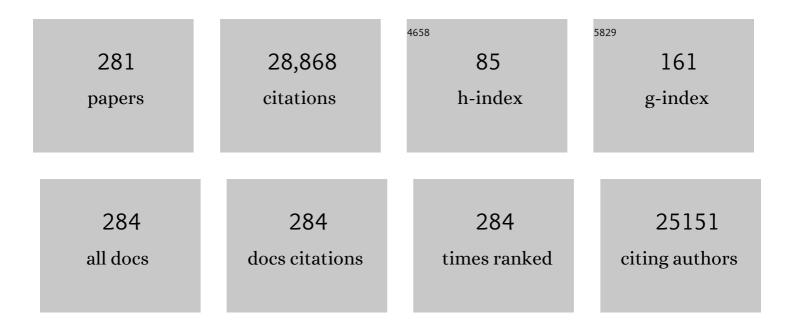
## Jin-Long Zhang

List of Publications by Year in descending order

Source: https://exaly.com/author-pdf/3034323/publications.pdf Version: 2024-02-01



#	Article	IF	CITATIONS
1	Understanding TiO <sub>2</sub> Photocatalysis: Mechanisms and Materials. Chemical Reviews, 2014, 114, 9919-9986.	47.7	4,658
2	Synthesis and Characterization of Nitrogen-Doped TiO2Nanophotocatalyst with High Visible Light Activity. Journal of Physical Chemistry C, 2007, 111, 6976-6982.	3.1	943
3	Mesoporous TiO <sub>2</sub> Nanocrystals Grown in Situ on Graphene Aerogels for High Photocatalysis and Lithium-Ion Batteries. Journal of the American Chemical Society, 2014, 136, 5852-5855.	13.7	745
4	Metal Sulfides as Excellent Co-catalysts for H2O2 Decomposition in Advanced Oxidation Processes. CheM, 2018, 4, 1359-1372.	11.7	679
5	Development of modified N doped TiO2 photocatalyst with metals, nonmetals and metal oxides. Energy and Environmental Science, 2010, 3, 715.	30.8	593
6	Characterization of Fe–TiO2 photocatalysts synthesized by hydrothermal method and their photocatalytic reactivity for photodegradation of XRG dye diluted in water. Journal of Molecular Catalysis A, 2004, 216, 35-43.	4.8	496
7	Singlet Oxygen Triggered by Superoxide Radicals in a Molybdenum Cocatalytic Fenton Reaction with Enhanced REDOX Activity in the Environment. Environmental Science & Technology, 2019, 53, 9725-9733.	10.0	465
8	Efficient Solar Light Harvesting CdS/Co <sub>9</sub> S <sub>8</sub> Hollow Cubes for Zâ€5cheme Photocatalytic Water Splitting. Angewandte Chemie - International Edition, 2017, 56, 2684-2688.	13.8	445
9	Fe3+-TiO2 photocatalysts prepared by combining sol–gel method with hydrothermal treatment and their characterization. Journal of Photochemistry and Photobiology A: Chemistry, 2006, 180, 196-204.	3.9	436
10	Recent advances in three-dimensional graphene based materials for catalysis applications. Chemical Society Reviews, 2018, 47, 2165-2216.	38.1	412
11	Preparation of Controllable Crystalline Titania and Study on the Photocatalytic Properties. Journal of Physical Chemistry B, 2005, 109, 8673-8678.	2.6	404
12	Size-dependent activity and selectivity of carbon dioxide photocatalytic reduction over platinum nanoparticles. Nature Communications, 2018, 9, 1252.	12.8	396
13	Preparation of Fe3+-doped TiO2 catalysts by controlled hydrolysis of titanium alkoxide and study on their photocatalytic activity for methyl orange degradation. Journal of Hazardous Materials, 2008, 155, 572-579.	12.4	323
14	Designing 3Dâ€MoS <sub>2</sub> Sponge as Excellent Cocatalysts in Advanced Oxidation Processes for Pollutant Control. Angewandte Chemie - International Edition, 2020, 59, 13968-13976.	13.8	316
15	Enhancement of H <sub>2</sub> O <sub>2</sub> Decomposition by the Co-catalytic Effect of WS <sub>2</sub> on the Fenton Reaction for the Synchronous Reduction of Cr(VI) and Remediation of Phenol. Environmental Science & Technology, 2018, 52, 11297-11308.	10.0	315
16	An economic method to prepare vacuum activated photocatalysts with high photo-activities and photosensitivities. Chemical Communications, 2011, 47, 4947.	4.1	308
17	Self-doped Ti 3+ -enhanced TiO 2 nanoparticles with a high-performance photocatalysis. Journal of Catalysis, 2013, 297, 236-243.	6.2	266
18	A new approach to prepare Ti3+ self-doped TiO2 via NaBH4 reduction and hydrochloric acid treatment. Applied Catalysis B: Environmental, 2014, 160-161, 240-246.	20.2	254

#	Article	IF	CITATIONS
19	Improved SERS Sensitivity on Plasmon-Free TiO <sub>2</sub> Photonic Microarray by Enhancing Light-Matter Coupling. Journal of the American Chemical Society, 2014, 136, 9886-9889.	13.7	252
20	New approaches to prepare nitrogen-doped TiO2 photocatalysts and study on their photocatalytic activities in visible light. Applied Catalysis B: Environmental, 2009, 89, 563-569.	20.2	247
21	Spatially Separated CdS Shells Exposed with Reduction Surfaces for Enhancing Photocatalytic Hydrogen Evolution. Advanced Functional Materials, 2017, 27, 1702624.	14.9	238
22	Constructing an Acidic Microenvironment by MoS <sub>2</sub> in Heterogeneous Fenton Reaction for Pollutant Control. Angewandte Chemie - International Edition, 2021, 60, 17155-17163.	13.8	237
23	Facile synthesis of the Ti3+ self-doped TiO2-graphene nanosheet composites with enhanced photocatalysis. Scientific Reports, 2015, 5, 8591.	3.3	235
24	Developing stretchable and graphene-oxide-based hydrogel for the removal of organic pollutants and metal ions. Applied Catalysis B: Environmental, 2018, 222, 146-156.	20.2	231
25	Emerging Cocatalysts on g <sub>3</sub> N <sub>4</sub> for Photocatalytic Hydrogen Evolution. Small, 2021, 17, e2101070.	10.0	223
26	Modifications on reduced titanium dioxide photocatalysts: A review. Journal of Photochemistry and Photobiology C: Photochemistry Reviews, 2017, 32, 21-39.	11.6	221
27	Ga-Doped and Pt-Loaded Porous TiO <sub>2</sub> –SiO <sub>2</sub> for Photocatalytic Nonoxidative Coupling of Methane. Journal of the American Chemical Society, 2019, 141, 6592-6600.	13.7	218
28	Ecofriendly Synthesis and Photocatalytic Activity of Uniform Cubic Ag@AgCl Plasmonic Photocatalyst. Journal of Physical Chemistry C, 2013, 117, 213-220.	3.1	217
29	Z-Scheme BiOCl-Au-CdS Heterostructure with Enhanced Sunlight-Driven Photocatalytic Activity in Degrading Water Dyes and Antibiotics. ACS Sustainable Chemistry and Engineering, 2017, 5, 6958-6968.	6.7	216
30	Yolk-shell structured Fe3O4@void@TiO2 as a photo-Fenton-like catalyst for the extremely efficient elimination of tetracycline. Applied Catalysis B: Environmental, 2017, 200, 484-492.	20.2	216
31	One step activation of WOx/TiO2 nanocomposites with enhanced photocatalytic activity. Applied Catalysis B: Environmental, 2009, 91, 397-405.	20.2	213
32	Synthesis and characterization of thermally stable Sm,N co-doped TiO2 with highly visible light activity. Journal of Hazardous Materials, 2010, 182, 386-393.	12.4	213
33	Photocatalytic Oxidation of Ethylene to CO2 and H2O on Ultrafine Powdered TiO2 Photocatalysts in the Presence of O2 and H2O. Journal of Catalysis, 1999, 185, 114-119.	6.2	211
34	Molybdenum sulfide Co-catalytic Fenton reaction for rapid and efficient inactivation of Escherichia coli. Water Research, 2018, 145, 312-320.	11.3	192
35	Ultrathin g-C3N4 nanosheet with hierarchical pores and desirable energy band for highly efficient H2O2 production. Applied Catalysis B: Environmental, 2020, 267, 118396.	20.2	183
36	Photo-Fenton degradation of phenol by CdS/rGO/Fe2+ at natural pH with in situ-generated H2O2. Applied Catalysis B: Environmental, 2019, 241, 367-374.	20.2	174

#	Article	IF	CITATIONS
37	Enhanced catalytic degradation of AO7 in the CeO2–H2O2 system with Fe3+ doping. Applied Catalysis B: Environmental, 2010, 101, 160-168.	20.2	168
38	Modulation of the Reduction Potential of TiO <sub>2–<i>x</i></sub> by Fluorination for Efficient and Selective CH <sub>4</sub> Generation from CO <sub>2</sub> Photoreduction. Nano Letters, 2018, 18, 3384-3390.	9.1	166
39	Surface modification of TiO2 with g-C3N4 for enhanced UV and visible photocatalytic activity. Journal of Alloys and Compounds, 2015, 631, 328-334.	5.5	157
40	Core–Shell Structural CdS@SnO <sub>2</sub> Nanorods with Excellent Visible-Light Photocatalytic Activity for the Selective Oxidation of Benzyl Alcohol to Benzaldehyde. ACS Applied Materials & Interfaces, 2015, 7, 13849-13858.	8.0	156
41	Highly-dispersed Boron-doped Graphene Nanosheets Loaded with TiO2 Nanoparticles for Enhancing CO2 Photoreduction. Scientific Reports, 2014, 4, 6341.	3.3	156
42	Plasmonic MoO <sub>3â^'x</sub> @MoO <sub>3</sub> nanosheets for highly sensitive SERS detection through nanoshell-isolated electromagnetic enhancement. Chemical Communications, 2016, 52, 2893-2896.	4.1	154
43	Singleâ€Atom Pt Loaded Zinc Vacancies ZnO–ZnS Induced Typeâ€V Electron Transport for Efficiency Photocatalytic H <sub>2</sub> Evolution. Solar Rrl, 2021, 5, 2100536.	5.8	153
44	Platinum Single Atoms Anchored on a Covalent Organic Framework: Boosting Active Sites for Photocatalytic Hydrogen Evolution. ACS Catalysis, 2021, 11, 13266-13279.	11.2	149
45	One-step preparation, characterization and visible-light photocatalytic activity of Cr-doped TiO2 with anatase and rutile bicrystalline phases. Chemical Engineering Journal, 2012, 191, 402-409.	12.7	139
46	Carbon nitride coupled Ti-SBA15 catalyst for visible-light-driven photocatalytic reduction of Cr (VI) and the synergistic oxidation of phenol. Applied Catalysis B: Environmental, 2017, 201, 1-11.	20.2	139
47	Self-modified breaking hydrogen bonds to highly crystalline graphitic carbon nitrides nanosheets for drastically enhanced hydrogen production. Applied Catalysis B: Environmental, 2018, 232, 306-313.	20.2	137
48	Efficient Fe(III)/Fe(II) cycling triggered by MoO2 in Fenton reaction for the degradation of dye molecules and the reduction of Cr(VI). Chinese Chemical Letters, 2019, 30, 2205-2210.	9.0	137
49	Sandwich-structured AgCl@Ag@TiO2 with excellent visible-light photocatalytic activity for organic pollutant degradation and E. coli K12 inactivation. Applied Catalysis B: Environmental, 2014, 158-159, 76-84.	20.2	132
50	An advanced TiO2/Fe2TiO5/Fe2O3 triple-heterojunction with enhanced and stable visible-light-driven fenton reaction for the removal of organic pollutants. Applied Catalysis B: Environmental, 2017, 211, 157-166.	20.2	127
51	Stöber-like method to synthesize ultradispersed Fe 3 O 4 nanoparticles on graphene with excellent Photo-Fenton reaction and high-performance lithium storage. Applied Catalysis B: Environmental, 2016, 183, 216-223.	20.2	125
52	Carbon dots modified mesoporous organosilica as an adsorbent for the removal of 2,4-dichlorophenol and heavy metal ions. Journal of Materials Chemistry A, 2015, 3, 13357-13364.	10.3	124
53	In situ growth of TiO <sub>2</sub> nanocrystals on g-C <sub>3</sub> N <sub>4</sub> for enhanced photocatalytic performance. Physical Chemistry Chemical Physics, 2015, 17, 17406-17412.	2.8	122
54	Recent Progress of Metal Sulfide Photocatalysts for Solar Energy Conversion. Advanced Materials, 2022, 34, .	21.0	122

#	Article	IF	CITATIONS
55	Bismuthâ€Doped Ordered Mesoporous TiO <sub>2</sub> : Visibleâ€Light Catalyst for Simultaneous Degradation of Phenol and Chromium. Chemistry - A European Journal, 2010, 16, 13795-13804.	3.3	121
56	Improving the thermal stability and photocatalytic activity of nanosized titanium dioxide via La3+ and N co-doping. Applied Catalysis B: Environmental, 2011, 101, 376-381.	20.2	118
57	Well-designed Ag/ZnO/3D graphene structure for dye removal: Adsorption, photocatalysis and physical separation capabilities. Journal of Colloid and Interface Science, 2019, 537, 66-78.	9.4	118
58	Ratiometric pH sensor based on mesoporous silica nanoparticles and Förster resonance energy transfer. Chemical Communications, 2010, 46, 8445.	4.1	115
59	Synergistic effect on the visible light activity of Ti3+ doped TiO2 nanorods/boron doped graphene composite. Scientific Reports, 2014, 4, 5493.	3.3	114
60	Fabrication of TiO2/Co-g-C3N4 heterojunction catalyst and its photocatalytic performance. Catalysis Communications, 2017, 89, 125-128.	3.3	113
61	Electron directed migration cooperated with thermodynamic regulation over bimetallic NiFeP/g-C3N4 for enhanced photocatalytic hydrogen evolution. Applied Catalysis B: Environmental, 2019, 259, 118078.	20.2	113
62	Enhanced photocatalytic performance of TiO2 based on synergistic effect of Ti3+ self-doping and slow light effect. Applied Catalysis B: Environmental, 2014, 160-161, 621-628.	20.2	111
63	Eco-friendly one-pot synthesis of well-adorned mesoporous g-C <sub>3</sub> N <sub>4</sub> with efficiently enhanced visible light photocatalytic activity. Catalysis Science and Technology, 2017, 7, 1726-1734.	4.1	111
64	Robust Photocatalytic H <sub>2</sub> O <sub>2</sub> Production over Inverse Opal g-C <sub>3</sub> N <sub>4</sub> with Carbon Vacancy under Visible Light. ACS Sustainable Chemistry and Engineering, 2019, 7, 16467-16473.	6.7	110
65	Singlet oxygen triggered by robust bimetallic MoFe/TiO2 nanospheres of highly efficacy in solar-light-driven peroxymonosulfate activation for organic pollutants removal. Applied Catalysis B: Environmental, 2021, 286, 119930.	20.2	110
66	Efficient Solar Light Harvesting CdS/Co <sub>9</sub> S <sub>8</sub> Hollow Cubes for Zâ€6cheme Photocatalytic Water Splitting. Angewandte Chemie, 2017, 129, 2728-2732.	2.0	108
67	Enhanced Photocatalysis by Au Nanoparticle Loading on TiO <sub>2</sub> Single-Crystal (001) and (110) Facets. Journal of Physical Chemistry Letters, 2013, 4, 3910-3917.	4.6	105
68	Integration of redox cocatalysts for artificial photosynthesis. Energy and Environmental Science, 2021, 14, 5260-5288.	30.8	105
69	Stöber-like method to synthesize ultralight, porous, stretchable Fe <sub>2</sub> O <sub>3</sub> /graphene aerogels for excellent performance in photo-Fenton reaction and electrochemical capacitors. Journal of Materials Chemistry A, 2015, 3, 12820-12827.	10.3	104
70	Study of Synergistic Effect of Ce- and S-Codoping on the Enhancement of Visible-Light Photocatalytic Activity of TiO <sub>2</sub> . Journal of Physical Chemistry C, 2013, 117, 9520-9528.	3.1	103
71	A robust and efficient catalyst of Cd <sub>x</sub> Zn <sub>1â^'x</sub> Se motivated by CoP for photocatalytic hydrogen evolution under sunlight irradiation. Chemical Communications, 2017, 53, 897-900.	4.1	103
72	Synthesis and photocatalytic activity of graphene based doped TiO2 nanocomposites. Applied Surface Science, 2014, 319, 8-15.	6.1	102

#	Article	IF	CITATIONS
73	Z-scheme CdS–Au–BiVO <sub>4</sub> with enhanced photocatalytic activity for organic contaminant decomposition. Catalysis Science and Technology, 2017, 7, 124-132.	4.1	102
74	Carbon nitride nanotubes with in situ grafted hydroxyl groups for highly efficient spontaneous H2O2 production. Applied Catalysis B: Environmental, 2021, 288, 119993.	20.2	102
75	The preparation, and applications of g-C3N4/TiO2 heterojunction catalysts—a review. Research on Chemical Intermediates, 2017, 43, 2081-2101.	2.7	100
76	0D/2D plasmonic Cu2-xS/g-C3N4 nanosheets harnessing UV-vis-NIR broad spectrum for photocatalytic degradation of antibiotic pollutant. Applied Catalysis B: Environmental, 2020, 263, 118326.	20.2	100
77	A Brown Mesoporous TiO <sub>2â€x</sub> /MCF Composite with an Extremely High Quantum Yield of Solar Energy Photocatalysis for H <sub>2</sub> Evolution. Small, 2015, 11, 1920-1929.	10.0	99
78	Controllable synthesis of graphitic carbon nitride nanomaterials for solar energy conversion and environmental remediation: the road travelled and the way forward. Catalysis Science and Technology, 2018, 8, 4576-4599.	4.1	99
79	Z-scheme photo-Fenton system for efficiency synchronous oxidation of organic contaminants and reduction of metal ions. Applied Catalysis B: Environmental, 2020, 279, 119365.	20.2	97
80	One-step large-scale highly active g-C <sub>3</sub> N <sub>4</sub> nanosheets for efficient sunlight-driven photocatalytic hydrogen production. Dalton Transactions, 2017, 46, 10678-10684.	3.3	92
81	Highly-dispersed boron-doped graphene nanoribbons with enhanced conductibility and photocatalysis. Chemical Communications, 2014, 50, 6637-6640.	4.1	91
82	Mesoporous graphitic carbon nitride materials: synthesis and modifications. Research on Chemical Intermediates, 2016, 42, 3979-3998.	2.7	91
83	Synthesis of core-shell structured CdS@CeO 2 and CdS@TiO 2 composites and comparison of their photocatalytic activities for the selective oxidation of benzyl alcohol to benzaldehyde. Catalysis Today, 2017, 281, 181-188.	4.4	91
84	Synthesis of Yolk–Shell Structured Fe <sub>3</sub> O <sub>4</sub> @void@CdS Nanoparticles: A General and Effective Structure Design for Photo-Fenton Reaction. ACS Applied Materials & Interfaces, 2016, 8, 20831-20838.	8.0	89
85	TiO2 inverse opal photonic crystals: Synthesis, modification, and applications - A review. Journal of Alloys and Compounds, 2018, 769, 740-757.	5.5	88
86	Metallic Active Sites on MoO2(110) Surface to Catalyze Advanced Oxidation Processes for Efficient Pollutant Removal. IScience, 2020, 23, 100861.	4.1	86
87	Wellâ€Dispersed Fe <sub>2</sub> O <sub>3</sub> Nanoparticles on g <sub>3</sub> N <sub>4</sub> for Efficient and Stable Photoâ€Fenton Photocatalysis under Visibleâ€Light Irradiation. European Journal of Inorganic Chemistry, 2016, 2016, 5387-5392.	2.0	85
88	Visibleâ€Lightâ€Driven Photocatalytic H <sub>2</sub> O <sub>2</sub> Production on g <sub>3</sub> N <sub>4</sub> Loaded with CoP as a Noble Metal Free Cocatalyst. European Journal of Inorganic Chemistry, 2017, 2017, 4797-4802.	2.0	84
89	Recent advances in visible light-responsive titanium oxide-based photocatalysts. Research on Chemical Intermediates, 2010, 36, 327-347.	2.7	82
90	Highly efficient photo-Fenton degradation of methyl orange facilitated by slow light effect and hierarchical porous structure of Fe2O3-SiO2 photonic crystals. Applied Catalysis B: Environmental, 2018, 237, 1160-1167.	20.2	82

#	Article	IF	CITATIONS
91	Hydrophobic Carbon-Doped TiO <sub>2</sub> /MCF-F Composite as a High Performance Photocatalyst. Journal of Physical Chemistry C, 2014, 118, 7329-7336.	3.1	81
92	Sustainable activation of peroxymonosulfate by the Mo(IV) in MoS2 for the remediation of aromatic organic pollutants. Chinese Chemical Letters, 2020, 31, 2803-2808.	9.0	81
93	Core–shell structured γ-Fe2O3@SiO2@AgBr:Ag composite with high magnetic separation efficiency and excellent visible light activity for acid orange 7 degradation. Applied Catalysis B: Environmental, 2014, 147, 22-28.	20.2	80
94	Dopant-Induced Edge and Basal Plane Catalytic Sites on Ultrathin C <sub>3</sub> N <sub>4</sub> Nanosheets for Photocatalytic Water Reduction. ACS Sustainable Chemistry and Engineering, 2020, 8, 7497-7502.	6.7	80
95	Improving the visible light photocatalytic activity of nano-sized titanium dioxide via the synergistic effects between sulfur doping and sulfation. Applied Catalysis B: Environmental, 2012, 115-116, 253-260.	20.2	79
96	Superoxide radicals dominated visible light driven peroxymonosulfate activation using molybdenum selenide (MoSe2) for boosting catalytic degradation of pharmaceuticals and personal care products. Applied Catalysis B: Environmental, 2021, 296, 120223.	20.2	78
97	Nonâ€oxidative Coupling of Methane: Nâ€ŧype Doping of Niobium Single Atoms in TiO <sub>2</sub> –SiO <sub>2</sub> Induces Electron Localization. Angewandte Chemie - International Edition, 2021, 60, 11901-11909.	13.8	77
98	Ultradispersed Cobalt Ferrite Nanoparticles Assembled in Graphene Aerogel for Continuous Photo-Fenton Reaction and Enhanced Lithium Storage Performance. Scientific Reports, 2016, 6, 29099.	3.3	75
99	Gel-hydrothermal synthesis of carbon and boron co-doped TiO2 and evaluating its photocatalytic activity. Journal of Hazardous Materials, 2011, 192, 368-73.	12.4	73
100	Oneâ€Step Hydrothermal Method to Prepare Carbon and Lanthanum Coâ€Doped TiO <sub>2</sub> Nanocrystals with Exposed {001} Facets and Their High UV and Visibleâ€Light Photocatalytic Activity. Chemistry - A European Journal, 2011, 17, 11432-11436.	3.3	72
101	Chiral Carbonaceous Nanotubes Modified with Titania Nanocrystals: Plasmonâ€Free and Recyclable SERS Sensitivity. Angewandte Chemie - International Edition, 2015, 54, 10643-10647.	13.8	72
102	Economic Hydrophobicity Triggering of CO <sub>2</sub> Photoreduction for Selective CH <sub>4</sub> Generation on Noble-Metal-Free TiO <sub>2</sub> –SiO <sub>2</sub> . Journal of Physical Chemistry Letters, 2016, 7, 2962-2966.	4.6	70
103	g-C3N4/CoAl-LDH 2D/2D hybrid heterojunction for boosting photocatalytic hydrogen evolution. International Journal of Hydrogen Energy, 2020, 45, 21331-21340.	7.1	70
104	Single-Atom High-Valent Fe(IV) for Promoted Photocatalytic Nitrogen Hydrogenation on Porous TiO <sub>2</sub> -SiO <sub>2</sub> . ACS Catalysis, 2021, 11, 4362-4371.	11.2	70
105	Facile phase control for hydrothermal synthesis of anatase-rutile TiO2 with enhanced photocatalytic activity. Journal of Alloys and Compounds, 2015, 646, 380-386.	5.5	69
106	Self-modification of g-C <sub>3</sub> N <sub>4</sub> with its quantum dots for enhanced photocatalytic activity. Catalysis Science and Technology, 2018, 8, 2617-2623.	4.1	69
107	Double-cocatalysts promote charge separation efficiency in CO <sub>2</sub> photoreduction: spatial location matters. Materials Horizons, 2016, 3, 608-612.	12.2	68
108	Synthesis of sandwich-structured AgBr@Ag@TiO 2 composite photocatalyst and study of its photocatalytic performance for the oxidation of benzyl alcohols to benzaldehydes. Chemical Engineering Journal, 2016, 306, 1151-1161.	12.7	67

#	Article	IF	CITATIONS
109	Hierarchical macro-mesoporous g-C <sub>3</sub> N <sub>4</sub> with an inverse opal structure and vacancies for high-efficiency solar energy conversion and environmental remediation. Nanoscale, 2019, 11, 20638-20647.	5.6	67
110	Visible Light-Driven Selective Organic Degradation by FeTiO3/Persulfate System: the Formation and Effect of High Valent Fe(IV). Applied Catalysis B: Environmental, 2021, 280, 119414.	20.2	67
111	High-efficiency adsorption of tetracycline by cooperation of carbon and iron in a magnetic Fe/porous carbon hybrid with effective Fenton regeneration. Applied Surface Science, 2021, 538, 147813.	6.1	67
112	Superbright Multifluorescent Coreâ^'Shell Mesoporous Nanospheres as Trackable Transport Carrier for Drug. ACS Nano, 2011, 5, 3447-3455.	14.6	66
113	Carbon Vacancy Mediated Incorporation of Ti <sub>3</sub> C <sub>2</sub> Quantum Dots in a 3D Inverse Opal g-C <sub>3</sub> N <sub>4</sub> Schottky Junction Catalyst for Photocatalytic H <sub>2</sub> O <sub>2</sub> Production. ACS Sustainable Chemistry and Engineering, 2021, 9, 481-488.	6.7	66
114	Exploring the Size Effect of Pt Nanoparticles on the Photocatalytic Nonoxidative Coupling of Methane. ACS Catalysis, 2021, 11, 3352-3360.	11.2	66
115	AgBr@Ag/TiO2 core–shell composite with excellent visible light photocatalytic activity and hydrothermal stability. Catalysis Communications, 2013, 38, 16-20.	3.3	64
116	A facile approach to further improve the substitution of nitrogen into reduced TiO2â^' with an enhanced photocatalytic activity. Applied Catalysis B: Environmental, 2015, 170-171, 66-73.	20.2	64
117	Mo0 and Mo4+ bimetallic reactive sites accelerating Fe2+/Fe3+ cycling for the activation of peroxymonosulfate with significantly improved remediation of aromatic pollutants. Chemosphere, 2020, 244, 125539.	8.2	63
118	Effect of surface fluorination on the photocatalytic and photo-induced hydrophilic properties of porous TiO2 films. Applied Surface Science, 2009, 255, 6290-6296.	6.1	62
119	Highly condensed g-C3N4-modified TiO2 catalysts with enhanced photodegradation performance toward acid orange 7. Journal of Materials Science, 2015, 50, 3467-3476.	3.7	62
120	Photocatalytic Performance of N-Doped TiO2 Adsorbed with Fe3+ Ions under Visible Light by a Redox Treatment. Journal of Physical Chemistry C, 2009, 113, 12848-12853.	3.1	61
121	Enhanced photocatalytic activities of vacuum activated TiO2 catalysts with Ti3+ and N co-doped. Catalysis Today, 2016, 266, 188-196.	4.4	61
122	Super-hydrophobic fluorination mesoporous MCF/TiO2 composite as a high-performance photocatalyst. Journal of Catalysis, 2012, 294, 37-46.	6.2	60
123	Preparation of high photocatalytic activity TiO2 with a bicrystalline phase containing anatase and TiO2 (B). Materials Letters, 2005, 59, 3378-3381.	2.6	58
124	Z-scheme inverse opal CN/BiOBr photocatalysts for highly efficient degradation of antibiotics. Physical Chemistry Chemical Physics, 2019, 21, 12818-12825.	2.8	58
125	Research progress of photocatalysis based on highly dispersed titanium in mesoporous SiO2. Chinese Chemical Letters, 2019, 30, 853-862.	9.0	58
126	Hollow Fe3O4/carbon with surface mesopores derived from MOFs for enhanced lithium storage performance. Science Bulletin, 2020, 65, 233-242.	9.0	58

#	Article	IF	CITATIONS
127	A colorimetric and ratiometric fluorescent probe for detection of palladium in the red light region. RSC Advances, 2015, 5, 52516-52521.	3.6	57
128	Nickel Boride Cocatalyst Boosting Efficient Photocatalytic Hydrogen Evolution Reaction. Industrial & Engineering Chemistry Research, 2018, 57, 8125-8130.	3.7	57
129	KOH-Assisted Band Engineering of Polymeric Carbon Nitride for Visible Light Photocatalytic Oxygen Reduction to Hydrogen Peroxide. ACS Sustainable Chemistry and Engineering, 2020, 8, 594-603.	6.7	57
130	An inverse opal TiO <sub>2</sub> /g-C <sub>3</sub> N <sub>4</sub> composite with a heterojunction for enhanced visible light-driven photocatalytic activity. Dalton Transactions, 2019, 48, 3486-3495.	3.3	56
131	Morphology-Controlled Synthesis and Applications of Silver Halide Photocatalytic Materials. Catalysis Surveys From Asia, 2012, 16, 210-230.	2.6	55
132	Multifluorescently Traceable Nanoparticle by a Single-Wavelength Excitation with Color-Related Drug Release Performance. Journal of the American Chemical Society, 2012, 134, 8746-8749.	13.7	54
133	Peroxymonosulfate activation by three-dimensional cobalt hydroxide/graphene oxide hydrogel for wastewater treatment through an automated process. Chemical Engineering Journal, 2020, 400, 125965.	12.7	54
134	Efficient degradation of antibiotics in different water matrices through the photocatalysis of inverse opal K-g-C3N4: Insights into mechanism and assessment of antibacterial activity. Chemical Engineering Journal, 2020, 400, 125902.	12.7	54
135	Fabrication of Co3O4 and Au co-modified BiOBr flower-like microspheres with high photocatalytic efficiency for sulfadiazine degradation. Separation and Purification Technology, 2020, 234, 116100.	7.9	52
136	Designing 3Dâ€MoS <sub>2</sub> Sponge as Excellent Cocatalysts in Advanced Oxidation Processes for Pollutant Control. Angewandte Chemie, 2020, 132, 14072-14080.	2.0	52
137	Reduced {001}-TiO <sub>2â^'x</sub> photocatalysts: noble-metal-free CO <sub>2</sub> photoreduction for selective CH <sub>4</sub> evolution. Physical Chemistry Chemical Physics, 2017, 19, 13875-13881.	2.8	50
138	Plasmon-free SERS self-monitoring of catalysis reaction on Au nanoclusters/TiO <sub>2</sub> photonic microarray. Chemical Communications, 2015, 51, 8813-8816.	4.1	49
139	Realization of all-in-one hydrogen-evolving photocatalysts via selective atomic substitution. Applied Catalysis B: Environmental, 2021, 298, 120518.	20.2	49
140	A colorimetric and ratiometric fluorescent probe with a large stokes shift for detection of hydrogen sulfide. Dyes and Pigments, 2015, 123, 78-84.	3.7	46
141	Study of synergistic effect of Sc and C co-doping on the enhancement of visible light photo-catalytic activity of TiO2. Applied Surface Science, 2016, 364, 446-454.	6.1	46
142	Yolk-shell structured composite for fast and selective lithium ion sieving. Journal of Colloid and Interface Science, 2018, 520, 33-40.	9.4	46
143	silver halide/silver iodide@silver composite with excellent visible light photocatalytic activity for methyl orange degradation. Journal of Colloid and Interface Science, 2013, 405, 17-21.	9.4	45
144	Carbon Dotâ€Incorporated PMO Nanoparticles as Versatile Platforms for the Design of Ratiometric Sensors, Multichannel Traceable Drug Delivery Vehicles, and Efficient Photocatalysts. Advanced Optical Materials, 2015, 3, 57-63.	7.3	45

#	Article	IF	CITATIONS
145	Graphene modified mesoporous titania single crystals with controlled and selective photoredox surfaces. Chemical Communications, 2016, 52, 1689-1692.	4.1	45
146	0D/3D coupling of g-C3N4 QDs/hierarchical macro-mesoporous CuO-SiO2 for high-efficiency norfloxacin removal in photo-Fenton-like processes. Journal of Hazardous Materials, 2021, 419, 126359.	12.4	45
147	Mesoporous silica-based carbon dot/TiO 2 photocatalyst for efficient organic pollutant degradation. Microporous and Mesoporous Materials, 2016, 226, 79-87.	4.4	44
148	Molybdenumâ€based heterogeneous catalysts for the control of environmental pollutants. EcoMat, 2021, 3, e12155.	11.9	44
149	Rational Design of a Unique Ternary Structure for Highly Photocatalytic Nitrobenzene Reduction. Journal of Physical Chemistry C, 2016, 120, 12125-12131.	3.1	43
150	Prolonged electron lifetime in sulfur vacancy-rich ZnCdS nanocages by interstitial phosphorus doping for photocatalytic water reduction. Materials Chemistry Frontiers, 2020, 4, 3234-3239.	5.9	42
151	Graphene Oxide-Supported Three-Dimensional Cobalt–Nickel Bimetallic Sponge-Mediated Peroxymonosulfate Activation for Phenol Degradation. ACS ES&T Engineering, 2021, 1, 1705-1714.	7.6	42
152	Cocatalytic Fenton Reaction for Pollutant Control. Cell Reports Physical Science, 2020, 1, 100149.	5.6	41
153	Double-diffusion-based synthesis of BiVO4 mesoporous single crystals with enhanced photocatalytic activity for oxygen evolution. Chemical Communications, 2016, 52, 7478-7481.	4.1	40
154	Reduced graphene oxide modified Ag/AgBr with enhanced visible light photocatalytic activity for methyl orange degradation. Chemical Physics Letters, 2013, 575, 81-85.	2.6	39
155	Facile Synthesis of Bimodal Mesoporous Fe3O4@SiO2Composite for Efficient Removal of Methylene Blue. European Journal of Inorganic Chemistry, 2015, 2015, 2928-2933.	2.0	39
156	Enhancing the photocatalytic activity of CdS nanorods for selective oxidation of benzyl alcohol by coating amorphous TiO2 shell layer. Catalysis Communications, 2015, 70, 30-33.	3.3	39
157	Operando SERS self-monitoring photocatalytic oxidation of aminophenol on TiO2 semiconductor. Applied Catalysis B: Environmental, 2018, 224, 305-309.	20.2	39
158	Formation of Highly Active Superoxide Sites on CuO Nanoclusters Encapsulated in SAPO-34 for Catalytic Selective Ammonia Oxidation. ACS Catalysis, 2019, 9, 10398-10408.	11.2	39
159	Facile one-pot synthesis of mesoporous g-C <sub>3</sub> N <sub>4</sub> nanosheets with simultaneous iodine doping and N-vacancies for efficient visible-light-driven H <sub>2</sub> evolution performance. Catalysis Science and Technology, 2020, 10, 549-559.	4.1	39
160	Recent advances of doped graphite carbon nitride for photocatalytic reduction of CO2: a review. Research on Chemical Intermediates, 2020, 46, 5133-5164.	2.7	39
161	Carbonâ€Dotâ€Sensitized, Nitrogenâ€Doped TiO <sub>2</sub> in Mesoporous Silica for Water Decontamination through Nonhydrophobic Enrichment–Degradation Mode. Chemistry - A European Journal, 2015, 21, 17944-17950.	3.3	38
162	Fluorine doped TiO2/mesocellular foams with an efficient photocatalytic activity. Catalysis Today, 2019, 327, 340-346.	4.4	38

#	Article	IF	CITATIONS
163	Mesoporous TiO2-B nanowires synthesized from tetrabutyl titanate. Journal of Physics and Chemistry of Solids, 2011, 72, 201-206.	4.0	37
164	"Small amount for multiple times―of H2O2 feeding way in MoS2-Fex heterogeneous fenton for enhancing sulfadiazine degradation. Chinese Chemical Letters, 2022, 33, 1365-1372.	9.0	37
165	Synthesis of mesoporous titania with high photocatalytic activity by nanocrystalline particle assembly. Microporous and Mesoporous Materials, 2006, 87, 177-184.	4.4	36
166	Regeneration of zero-valent iron powder by the cocatalytic effect of WS2 in the environmental applications. Chemical Engineering Journal, 2020, 383, 123158.	12.7	36
167	Synthesis of thermally stable and highly ordered bicontinuous cubic mesoporous titania–silica binary oxides with crystalline framework. Microporous and Mesoporous Materials, 2009, 126, 50-57.	4.4	35
168	Core-shell mesoporous silica nanospheres used as Zn2+ ratiometric fluorescent sensor and adsorbent. RSC Advances, 2012, 2, 2783.	3.6	35
169	Vacancy Engineering of Ultrathin 2D Materials for Photocatalytic CO <sub>2</sub> Reduction. ChemNanoMat, 2021, 7, 368-379.	2.8	35
170	AgBr tetradecahedrons with co-exposed {100} and {111} facets: simple fabrication and enhancing spatial charge separation using facet heterojunctions. Journal of Materials Chemistry A, 2016, 4, 18570-18577.	10.3	34
171	A binary polymer composite of graphitic carbon nitride and poly(diphenylbutadiyne) with enhanced visible light photocatalytic activity. RSC Advances, 2017, 7, 27377-27383.	3.6	34
172	Photo-fenton refreshable Fe3O4@HCS adsorbent for the elimination of tetracycline hydrochloride. Research on Chemical Intermediates, 2018, 44, 1-11.	2.7	34
173	Phosphorus-doped inverse opal g-C <sub>3</sub> N <sub>4</sub> for efficient and selective CO generation from photocatalytic reduction of CO <sub>2</sub> . Catalysis Science and Technology, 2020, 10, 3694-3700.	4.1	34
174	Preparation and characterization of nitrogen-doped TiO2 photocatalyst in different acid environments. Research on Chemical Intermediates, 2006, 32, 717-724.	2.7	33
175	Facile preparation of C-modified TiO <sub>2</sub> supported on MCF for high visible-light-driven photocatalysis. RSC Advances, 2015, 5, 17802-17808.	3.6	33
176	Facet-Heterojunction-Based Z-Scheme BiVO <sub>4</sub> {010} Microplates Decorated with AgBr-Ag Nanoparticles for the Photocatalytic Inactivation of Bacteria and the Decomposition of Organic Contaminants. ACS Applied Nano Materials, 2020, 3, 8604-8617.	5.0	33
177	Recent advances in photo-enhanced dry reforming of methane: A review. Journal of Photochemistry and Photobiology C: Photochemistry Reviews, 2022, 51, 100468.	11.6	33
178	One-step in situ green template mediated porous graphitic carbon nitride for efficient visible light photocatalytic activity. Journal of Environmental Chemical Engineering, 2017, 5, 3500-3507.	6.7	32
179	Fabrication of 3D Sponge@AgBr-AgCl/Ag and Tubular Photoreactor for Continuous Wastewater Purification under Sunlight Irradiation. ACS Sustainable Chemistry and Engineering, 2019, 7, 14051-14063.	6.7	32
180	Photocatalysis. Lecture Notes in Quantum Chemistry II, 2018, , .	0.3	32

#	Article	IF	CITATIONS
181	Silica nanocrystal/graphene composite with improved photoelectric and photocatalytic performance. Applied Catalysis B: Environmental, 2016, 180, 106-112.	20.2	31
182	The role of oxygen defects in metal oxides for CO <sub>2</sub> reduction. Nanoscale Advances, 2020, 2, 4986-4995.	4.6	31
183	Singlet oxygen mediated Fe2+/peroxymonosulfate photo-Fenton-like reaction driven by inverse opal WO3 with enhanced photogenerated charges. Chemical Engineering Journal, 2021, 425, 128644.	12.7	31
184	Visible-light-induced reduction of hexavalent chromium utilizing cobalt phosphate (Co-Pi) sensitized inverse opal TiO <sub>2</sub> as a photocatalyst. Catalysis Science and Technology, 2017, 7, 5687-5693.	4.1	30
185	TiO2 (B) nanotubes with ultrathin shell for highly efficient photocatalytic fixation of nitrogen. Catalysis Today, 2019, 335, 214-220.	4.4	30
186	Novel Fenton process of Co-catalyst Co9S8 quantum dots for highly efficient removal of organic pollutants. Chemosphere, 2021, 270, 128648.	8.2	30
187	Metal–Organic Framework MIL-101(Fe) Nanoparticles Decorated with Ag Nanoparticles for Regulating the Photocatalytic Phenol Oxidation Pathway for Cr(VI) Reduction. ACS Applied Nano Materials, 2021, 4, 4513-4521.	5.0	29
188	The evolvement of pits and dislocations on TiO2-B nanowires via oriented attachment growth. Journal of Solid State Chemistry, 2009, 182, 2225-2230.	2.9	28
189	Gold-loaded graphene oxide/PDPB composites for the synchronous removal of Cr(VI) and phenol. Chinese Journal of Catalysis, 2018, 39, 8-15.	14.0	28
190	Unidirectional/Bidirectional Electron Transfer at the Au/TiO <sub>2</sub> Interface Operando Tracked by SERS Spectra from Au and TiO <sub>2</sub> . ACS Applied Materials & Interfaces, 2021, 13, 16498-16506.	8.0	28
191	Photo-Fenton-like degradation of antibiotics by inverse opal WO3 co-catalytic Fe2+/PMS, Fe2+/H2O2 and Fe2+/PDS processes: A comparative study. Chemosphere, 2022, 288, 132627.	8.2	27
192	Efficient removal of antibiotic-resistant bacteria and intracellular antibiotic resistance genes by heterogeneous activation of peroxymonosulfate on hierarchical macro-mesoporous Co3O4-SiO2 with enhanced photogenerated charges. Journal of Hazardous Materials, 2022, 430, 127414.	12.4	27
193	Synthesis of visible-light driven Cr O –TiO2 binary photocatalyst based on hierarchical macro–mesoporous silica. Applied Catalysis B: Environmental, 2015, 163, 9-15.	20.2	26
194	Preparation of NiCoP-decorated g-C3N4 as an efficient photocatalyst for H2O2 production. Research on Chemical Intermediates, 2019, 45, 5907-5917.	2.7	26
195	The photoluminescence of coumarin derivative encapsulated in MCM-41 and Ti-MCM-41. Dyes and Pigments, 2005, 64, 265-270.	3.7	24
196	Aim and shoot: molecule-imprinting polymer coated MoO <sub>3</sub> for selective SERS detection and photocatalytic destruction of low-level organic contaminants. RSC Advances, 2017, 7, 36201-36207.	3.6	24
197	Zn-Assisted TiO <sub>2–<i>x</i></sub> Photocatalyst with Efficient Charge Separation for Enhanced Photocatalytic Activities. Journal of Physical Chemistry C, 2017, 121, 17068-17076.	3.1	24
198	Carbon-doped titanum dioxide nanocrystals for highly efficient dye-sensitized solar cells. Catalysis Today, 2017, 281, 636-641.	4.4	24

#	Article	IF	CITATIONS
199	Enhanced photocatalytic CO2reduction to CH4over separated dual co-catalysts Au and RuO2. Nanotechnology, 2018, 29, 154005.	2.6	24
200	Gaseous bubble-assisted in-situ construction of worm-like porous g-C3N4 with superior visible light photocatalytic performance. Applied Catalysis A: General, 2019, 573, 13-21.	4.3	24
201	Photocatalytic non-oxidative coupling of methane: Recent progress and future. Journal of Photochemistry and Photobiology C: Photochemistry Reviews, 2021, 46, 100400.	11.6	24
202	Building of multifluorescent mesoporous silica nanoparticles. Chemical Communications, 2009, , 2195.	4.1	23
203	Preparation, characterization, and photocatalytic activity of porous AgBr@Ag and AgBrl@Ag plasmonic photocatalysts. Applied Surface Science, 2014, 292, 256-261.	6.1	23
204	The reduction behavior of the Cu ion species exchanged into Y zeolite during the thermovacuum treatment. Journal of Catalysis, 2004, 228, 75-79.	6.2	22
205	g-C3N4 quantum dots-modified mesoporous TiO2–SiO2 for enhanced photocatalysis. Research on Chemical Intermediates, 2019, 45, 4237-4247.	2.7	22
206	Recent Progress of Photocatalytic Fenton-Like Process for Environmental Remediation. Frontiers in Environmental Chemistry, 2020, 1, .	1.6	22
207	Chemisorptionâ€Induced and Plasmonâ€Promoted Photofixation of Nitrogen on Goldâ€Loaded Carbon Nitride Nanosheets. ChemSusChem, 2020, 13, 3455-3461.	6.8	22
208	A fluorescein-based fluorescence probe for the fast detection of thiol. Tetrahedron Letters, 2016, 57, 2478-2483.	1.4	21
209	A coumarin-based fluorescent probe for the fast detection of PdO with low detection limit. Tetrahedron Letters, 2016, 57, 1451-1455.	1.4	21
210	Vacuum activation-induced Ti3+ and carbon co-doped TiO2 with enhanced solar light photo-catalytic activity. Research on Chemical Intermediates, 2016, 42, 4181-4189.	2.7	21
211	A facile "polystyrene-dissolving―strategy to hollow periodic mesoporous organosilica with flexible structure-tailorability. Microporous and Mesoporous Materials, 2017, 239, 173-179.	4.4	21
212	Deep insight of the influence of Cu valence states in co-catalyst on CO2 photoreduction. Applied Catalysis B: Environmental, 2022, 316, 121621.	20.2	21
213	In situ strategy to prepare PDPB/SnO <sub>2</sub> p–n heterojunction with a high photocatalytic activity. RSC Advances, 2017, 7, 24064-24069.	3.6	20
214	Hollow-structured Fe2O3/Au/SiO2 nanorods with enhanced and recyclable photo-Fenton oxidation for the remediation of organic pollutants. Materials Today Chemistry, 2019, 11, 86-93.	3.5	20
215	Constructing an Acidic Microenvironment by MoS <sub>2</sub> in Heterogeneous Fenton Reaction for Pollutant Control. Angewandte Chemie, 2021, 133, 17292-17300.	2.0	20
216	A structural engineering-inspired CdS based composite for photocatalytic remediation of organic pollutant and hexavalent chromium. Catalysis Today, 2019, 335, 101-109.	4.4	19

#	Article	IF	CITATIONS
217	Dual-Shell Fluorescent Nanoparticles for Self-Monitoring of pH-Responsive Molecule-Releasing in a Visualized Way. ACS Applied Materials & Interfaces, 2016, 8, 19084-19091.	8.0	18
218	Single-step solvothermal synthesis of mesoporous anatase TiO2-reduced graphene oxide nanocomposites for the abatement of organic pollutants. Research on Chemical Intermediates, 2017, 43, 5187-5201.	2.7	18
219	Z-scheme structure SnS2–Au–CdS with excellent photocatalytic performance for simultaneous removal of Cr(VI) and methyl orange. Research on Chemical Intermediates, 2019, 45, 3513-3524.	2.7	18
220	Facet-heterojunction-based photothermocatalyst CdS-Au-{0 1 0}BiVO4{1 1 0}-MnOx with excellent synergetic effect for toluene degradation. Chemical Engineering Journal, 2022, 442, 135835.	12.7	18
221	High-efficiency electron tandem flow mode on carbon nitride/titanium dioxide heterojunction for visible light nitrogen photofixation. Chemical Engineering Journal, 2022, 443, 136425.	12.7	18
222	Sulfur nanoparticles in situ growth on TiO <sub>2</sub> mesoporous single crystals with enhanced solar light photocatalytic performance. RSC Advances, 2016, 6, 77863-77869.	3.6	17
223	Improving SERS sensitivity of TiO <sub>2</sub> by utilizing the heterogeneity of facet-potentials. Journal of Materials Chemistry C, 2020, 8, 13836-13842.	5.5	17
224	Synthesis and proton-induced fluorescence "OFF–ON―switching of a new D-ï€-A type pyran dye. Research on Chemical Intermediates, 2015, 41, 525-533.	2.7	16
225	Cobalt phosphide nanocages encapsulated with graphene as ultralong cycle life anodes for reversible lithium storage. Research on Chemical Intermediates, 2018, 44, 7847-7859.	2.7	16
226	gâ€C <sub>3</sub> N <sub>4</sub> Inverse Opals with Isotype Heterostructure for Enhanced Visibleâ€Lightâ€Driven Photocatalysis. Chemistry - an Asian Journal, 2018, 13, 3261-3267.	3.3	16
227	Advances for CO <sub>2</sub> Photocatalytic Reduction in Porous Ti-Based Photocatalysts. ACS ES&T Engineering, 2022, 2, 942-956.	7.6	16
228	A colorimetric and fluorescent chemodosimeter responding to Cu2+ with high selectivity and sensitivity. Research on Chemical Intermediates, 2015, 41, 5915-5927.	2.7	15
229	Self-assembly of magnetically recoverable ratiometric Cu <sup>2+</sup> fluorescent sensor and adsorbent. RSC Advances, 2014, 4, 18660-18667.	3.6	14
230	Hierarchically mesoporous/macroporous structured TiO <sub>2</sub> for dye-sensitized solar cells. RSC Advances, 2015, 5, 74557-74561.	3.6	14
231	Advanced Bi2O2.7/Bi2Ti2O7 composite film with enhanced visible-light-driven activity for the degradation of organic dyes. Research on Chemical Intermediates, 2018, 44, 4609-4618.	2.7	14
232	Auâ€Mediated Composite In <sub>2</sub> S <sub>3</sub> –Au–BiVO <sub>4</sub> with Enhanced Photocatalytic Activity for Organic Pollutant Degradation. ChemistrySelect, 2018, 3, 4889-4896.	1.5	14
233	Facile Fabrication of Amorphous Molybdenum Oxide as a Sensitive and Stable SERS Substrate under Redox Treatment. Chemistry - A European Journal, 2020, 26, 2653-2657.	3.3	14
234	Embedding [Mo3S13]2â^' clusters into the micropores of a covalent organic framework for enhanced stability and photocatalytic hydrogen evolution. Chemical Engineering Journal, 2022, 446, 136883.	12.7	14

#	Article	IF	CITATIONS
235	Fâ^ assistant synthesis of ultra-hydrothermally stable mesoporous silica by using nonionic organosilicon surfactant as templates. Microporous and Mesoporous Materials, 2009, 124, 204-209.	4.4	13
236	Titanate nanowire as a precursor for facile morphology control of TiO2 catalysts with enhanced photocatalytic activity. Journal of Alloys and Compounds, 2016, 687, 927-936.	5.5	13
237	Mesoporous silica-based carbon dot–carbon nitride composite for efficient photocatalysis. RSC Advances, 2017, 7, 52626-52631.	3.6	13
238	Synthesis of cubic Ag@AgCl and Ag@AgBr plasmonic photocatalysts and comparison of their photocatalytic activity for degradation of methyl orange and 2,4-dichlorophenol. Research on Chemical Intermediates, 2018, 44, 4651-4661.	2.7	13
239	Nonâ€oxidative Coupling of Methane: Nâ€type Doping of Niobium Single Atoms in TiO <sub>2</sub> –SiO <sub>2</sub> Induces Electron Localization. Angewandte Chemie, 2021, 133, 12008-12016.	2.0	13
240	Highly efficient photocatalytic H2O2 production on core–shell CdS@CdIn2S4 heterojunction in non-sacrificial system. Research on Chemical Intermediates, 2021, 47, 3379-3393.	2.7	13
241	Magnetic separation of metal sulfides/oxides by Fe3O4 at room temperature and atmospheric pressure. Rare Metals, 2019, 38, 379-389.	7.1	12
242	Design of frustrated Lewis pair in defective TiO2 for photocatalytic non-oxidative methane coupling. Chem Catalysis, 2022, 2, 1775-1792.	6.1	12
243	Study on the fluorescence properties of benzopyrylium salt in Ti-HMS. Dyes and Pigments, 2004, 63, 71-76.	3.7	11
244	Facile tailoring of titanate nanostructures at low alkaline concentration by a solvothermal route. Journal of Materials Science, 2012, 47, 3855-3866.	3.7	11
245	SERS self-monitoring of Ag-catalyzed reaction by magnetically separable mesoporous Fe 3 O 4 @Ag@mSiO 2. Microporous and Mesoporous Materials, 2018, 263, 113-119.	4.4	11
246	Selective Photocatalytic CO <sub>2</sub> Reduction to CH <sub>4</sub> on Tri- <i>s</i> -triazine-Based Carbon Nitride via Defects and Crystal Regulation: Synergistic Effect of Thermodynamics and Kinetics. ACS Applied Materials & Interfaces, 2022, 14, 25417-25426.	8.0	11
247	Synthesis of yolk-shell Fe3O4@void@CeO2 nanoparticles and their application in SERS. Applied Surface Science, 2021, 541, 148422.	6.1	10
248	Tuning Reaction Pathway of CO <sub>2</sub> Photoreduction via PtRu Bimetallic Microstructure Regulation. Journal of Physical Chemistry C, 2021, 125, 10406-10412.	3.1	10
249	Photo-generated charges escape from P+ center through the chemical bridges between P-doped g-C3N4 and RuxP nanoparticles to enhance the photocatalytic hydrogen evolution. Catalysis Today, 2021, 380, 223-229.	4.4	10
250	Fabrication of CuS-modified inverse opal g-C3N4 photocatalyst with enhanced performance of photocatalytic reduction of CO2. Journal of CO2 Utilization, 2021, 54, 101779.	6.8	10
251	Preparation of porous TiO <sub>2</sub> photocatalyts with different crystal phases and high catalytic activity by simple calcination of titanate nanofibers. RSC Advances, 2017, 7, 45742-45745.	3.6	9
252	Enhanced photoreduction of Cr( <scp>vi</scp> ) and photooxidation of NO over TiO <sub>2â^'x</sub> mesoporous single crystals. RSC Advances, 2017, 7, 55927-55934.	3.6	9

#	Article	IF	CITATIONS
253	Graphene-Based Photo-Fenton Catalysts for Pollutant Control. Transactions of Tianjin University, 2021, 27, 110-126.	6.4	9
254	Carbon Nitride Quantum Dots Modified TiO2 Inverse Opal Photonic Crystal for Solving Indoor VOCs Pollution. Catalysts, 2021, 11, 464.	3.5	9
255	S-Scheme BiOCl/MoSe2 Heterostructure with Enhanced Photocatalytic Activity for Dyes and Antibiotics Degradation under Sunlight Irradiation. Sensors, 2022, 22, 3344.	3.8	9
256	Fluorinated inverse opal carbon nitride combined with vanadium pentoxide as a Z-scheme photocatalyst with enhanced photocatalytic activity. Chinese Chemical Letters, 2022, 33, 3797-3801.	9.0	8
257	Ammonium acetate and ethylenediamine-assisted synthesis of anatase nanocrystals with {010} facets and enhanced photocatalytic activity. Journal of Environmental Chemical Engineering, 2015, 3, 961-968.	6.7	7
258	αâ€FeOOHâ^'MoO <sub>3</sub> Nanorod for Effective Photoâ€Fenton Degradation of Dyes and Antibiotics at a Wide Range of pH. Chemistry - an Asian Journal, 2020, 15, 2749-2753.	3.3	7
259	Is g-C3N4 more suitable for photocatalytic reduction or oxidation in environmental applications?. , 2022, 1, 121-125.		7
260	Construction of Cu cocatalyst on TiO2 for regulating the selectivity of photocatalytic CO2 reduction. Research on Chemical Intermediates, 2022, 48, 3275-3287.	2.7	7
261	The synthesis and fluorescence properties of novel 1,8-naphthalimide derivatives. Research on Chemical Intermediates, 2015, 41, 1157-1169.	2.7	6
262	Hierarchical porous TiO2 single crystals templated from partly glassified polystyrene. Journal of Colloid and Interface Science, 2019, 538, 248-255.	9.4	6
263	Controllable Synthesis of Inverse Opal TiO <sub>2â€<i>x</i></sub> Photonic Crystals and Their Photoelectric Properties. Chemistry - an Asian Journal, 2019, 14, 322-327.	3.3	6
264	Exploring the slow-light effect of Pt/TiO <sub>2</sub> –SiO <sub>2</sub> inverse opal on photocatalytic nonoxidative coupling of methane. Chemical Communications, 2021, 57, 13000-13003.	4.1	6
265	Highly Dispersed Cobalt Centers on UiO-66-NH2 for Photocatalytic CO2 Reduction. Catalysis Letters, 2023, 153, 1475-1482.	2.6	6
266	Enhanced Visible Light Photocatalytic Activity of Flowerâ€Like <scp>Bi<sub>2</sub>WO<sub>6</sub></scp> Loaded with MnO <i><sub>x</sub></i> . Chinese Journal of Chemistry, 2017, 35, 153-158.	4.9	5
267	TiO2/carbon composite nanomaterials for photocatalysis. , 2020, , 303-321.		5
268	MoO <sub>3</sub> -modified SAPO-34 for photocatalytic nonoxidative coupling of methane. Catalysis Science and Technology, 2022, 12, 3322-3327.	4.1	5
269	Au thorn-decorated TiO2 hierarchical microspheres with superior photocatalytic bactericidal activity under red and NIR light irradiation. Journal of Alloys and Compounds, 2022, 910, 164485.	5.5	5
270	The effect of silver resources on the photocatalytic reduction and oxidation properties of AgSCN. Materials Technology, 2017, 32, 852-861.	3.0	4

#	Article	IF	CITATIONS
271	Molybdenum oxide nanorods decorated with molybdenum phosphide quantum dots for efficient photocatalytic degradation of rhodamine B and norfloxacin. Research on Chemical Intermediates, 2022, 48, 2887-2901.	2.7	4
272	Syntheses and Applications of Silver Halide-Based Photocatalysts. Lecture Notes in Quantum Chemistry II, 2018, , 307-343.	0.3	3
273	Photothermocatalytic System Designed by Facetâ€heterojunction to Enhance the Synergistic Effect of Toluene Oxidation. ChemCatChem, 2022, 14, .	3.7	3
274	Application of defective TiO2 inverse opal in photocatalytic non-oxidative CH4 coupling. Research on Chemical Intermediates, 2022, 48, 3247-3258.	2.7	3
275	Transition Metal Phosphide As Cocatalysts for Semiconductor-Based Photocatalytic Hydrogen Evolution Reaction. Lecture Notes in Quantum Chemistry II, 2018, , 375-402.	0.3	2
276	Heterogeneous Photo-Fenton Technology. Lecture Notes in Quantum Chemistry II, 2018, , 241-258.	0.3	2
277	The Preparation and Applications of g-C3N4/TiO2 Heterojunction Catalysts. Lecture Notes in Quantum Chemistry II, 2018, , 173-196.	0.3	2
278	Preparation of Reduced TiO2–x for Photocatalysis. Lecture Notes in Quantum Chemistry II, 2018, , 75-105.	0.3	1
279	Photo-Fenton Reaction. Lecture Notes in Quantum Chemistry II, 2018, , 259-274.	0.3	1
280	Synthesis of nitrogen and terbium co-doped TiO <sub>2</sub> nanocrystals with enhanced photocatalytic activity for AO7 degradation under visible-light radiation. New Journal of Chemistry, 2022, 46, 6878-6884.	2.8	1
281	Synthesis of Yolk-Shell Structured Fe3O4@Void@CdS Nanoparticles: A General and Effective Structure Design for Photo-Fenton Reaction. Nanostructure Science and Technology, 2021, , 459-478.	0.1	Ο